# PHASE DIAGRAM OF GRAPHENE IN THE PRESENCE OF SPIN-ORBIT COUPLING AND ELECTRON-ELECTRON INTERACTION

**Phung Thi Thu[1,2]\*, Nguyen Thi Mai[3], Pham Thi Lien[3], Nguyen Thanh Tung[3], Ngo Thi Lan[4]**

[1]*Graduate University of Science and Technology - Vietnam Academy of Science and Technology*
[2]*University of Science and Technology of Hanoi - Vietnam Academy of Science and Technology*
[3]*Institute of Materials Sciences - Vietnam Academy of Science and Technology*
[4]*TNU – Thai Nguyen University of Sciences*

\*Corresponding author: thuphungi2@gmail.com

**Abstract -** We theoretically investigate in this work the interplay between the intrinsic spin-orbit coupling (SOC) and electron-electron interaction on the magnetism in the graphene honeycomb lattice. Particularly, a phase diagram is here explored and studied by Kane-Mele-Hubbard (KMH) model combined with mean-field theory and self-consistent algorithm. Results show that the graphene undergoes a phase transition from the gapless semi-metal to topological band insulator (TBI) at a finite SOC and weak Coulomb energy $U$, and another transition from the TBI to antiferromagnetic ordered insulator at stronger Coulomb energy $U$ observed as well. Moreover, our calculations also point out the prior developing orientation of magnetic moments in the in-plane direction driven by the SOC rather than that in the out-of-plane direction without the SOC.

**Key words -** Graphene; Kane-Mele-Hubbard (KMH) model; mean-field theory; phase diagram; magnetism.

## 1. Introduction

Together with the progress in fabricating technology, two-dimensional graphene and its derivatives have opened a new era by the presence in many domains from industry to human living on account of its intriguing properties. Graphene is constructed by $sp^2$ hybridized carbon atoms arranged in the honeycomb lattice. The graphene possesses a unique electronic band structure, and can be thus described by the Dirac equation for the massless fermions at low energy [1]. Its impressive properties should be listed such as the absence of backscattering originated from the conservation of pseudospin, high thermal conductivity and mobility, large surface area, good biocompatibility, non-toxicity... [1 - 3]. Despite the absence of $d$ and $f$ electrons, a magnetic state in the graphene can be triggered by introducing vacancies, dopants, edge structures or hydrogenation, therefore the graphene is one of excellent candidates in spintronics and spin caloritronics [4, 5]. Unlike the non-magnetic graphene bulk, graphene nanostructures manifest an exotic magnetism with the ground-state antiferromagnetic order [6 - 8]. Theoretically, the magnetic state can be found in the graphene bulk as introducing a strong Coulomb energy using the Hubbard model [9]. Both the theory and experiment have confirmed the spin polarization localized at the zigzag edge of graphene nanoribbons, and a transition from the antiferromagnetism at ground-state to the ferromagnetism at excited states have been also observed [4, 10]. These results are due to the electronic states localized at the zigzag edges which do not exist in the armchair edges [4].

As a consequence, no spin polarization is expected for the armchair edges. Most interestingly, it can be tuned not only the electronic band structure but also magnetization of graphene by size and geometry [6, 11]. In addition, strain, doping and defects such as vacancies also are factors resulting in the modification of magnetic properties in graphene nanostructure [12 - 14].

Noticeably, spin-orbit interaction giving rise to a nontrivial topological band insulator has recently attracted much attention. A topological insulator is characterized by opening a bulk gap, the edge helical states and the time reversal symmetry [15]. Kane-Mele model [16] was proposed in order to account for the SOC for the honeycomb lattice based on earlier work of Haldane [17]. In the presence of electron-electron interaction, KMH model has been studied using Quantum Monte Carlo (QMC), Mean-field theory (MFT), Variational cluster approach [15, 18 - 20]. Investigations have indicated the unstableness of topological insulating phase to the electron-electron interaction. The SOC also contributes to suppress the edge magnetism in the zigzag graphene nanoribbon [21]. Leong et al., [22] revealed the enhancement of localized spin moments near a single vacancy under affecting the SOC. The change of topological edge states and spontaneous magnetic moment properties of zigzag graphene nanoribbons were reported recently [23]. Furthermore, so far, the graphene honeycomb lattice has become a fundamental research subject in condensed matter physics to exploit novel features in the 2D materials and hence enhance the further possibility of application in nano-devices.

In this work, we investigate and numerically calculate the interplay between the SOC and electron-electron interactions on the magnetic properties of the graphene honeycomb lattice using the KMH model within the Hartree - Fock approximation. The purposes of this paper are the description of the Hartree -Fock approximation for the KMH model and the discussion of the phase diagram when invoking both Hartree and Fock terms which have yet to report.

## 2. Methodology

Given problem in this study is addressed by the KMH model combined with the Hartree - Fock approximation. The KMH Hamiltonian is constructed by three terms as follows;

$$H = -t \sum_{\langle i,j \rangle} (a_{i\sigma}^+ b_{j\sigma} + b_{j\sigma}^+ a_{i\sigma})$$
$$+ i\lambda \sum_{\langle\langle i,j \rangle\rangle} \sum_{\sigma\sigma'} v_{ij} \sigma_{\sigma\sigma'}^z (a_{i\sigma}^+ a_{j\sigma'} + b_{i\sigma}^+ b_{j\sigma'}) + U \sum_i n_{i\uparrow} n_{i\downarrow}.$$

$$(1)$$

Where $a_{i\sigma}^+$ and $b_{i\sigma}$ are creation and annihilation operators of the $A$ and $B$ sublattices for spin at site $i$, respectively, because the graphene has bipartite lattice structure. Each unit cell consists of two carbon atoms belonging to two different sublattices $A$ and $B$. The first term describes the nearest hoping tight-binding with the nearest-neighbor hopping amplitude $t$ (set up = 1 in our calculation). The second term represents the spin-orbit interaction in which $\lambda$ and $\sigma_{\sigma\sigma'}^z$ are SOC amplitude and Pauli matrix, respectively, and $v_{ij}$ is related to the orientation of sites (giving "+" for clockwise and "-" for anticlockwise). The final term, well-known as Hubbard one ($H_U$), introduces the electron-electron interaction with Coulomb energy $U$ and spin-resolved density operators at site $i$ for spin $\sigma$, $n_{i\sigma} = a_{i\sigma}^+ a_{i\sigma}$ ($n_{i\sigma} = b_{i\sigma}^+ b_{i\sigma}$).

The MFT was next applied to treat the electron-electron interaction in the KMH Hamiltonian. In particular, the spin-resolved density operators can be expressed as follows:

$$n_{i\uparrow} = \langle n_{i\uparrow} \rangle + (n_{i\uparrow} - \langle n_{i\uparrow} \rangle),$$
$$n_{i\downarrow} = \langle n_{i\downarrow} \rangle + (n_{i\downarrow} - \langle n_{i\downarrow} \rangle). \quad (2)$$

After several mathematical calculations and concurrently ignoring a very small deviation, one gets

$$n_{i\uparrow} n_{i\downarrow} = \langle n_{i\downarrow} \rangle n_{i\uparrow} + \langle n_{i\uparrow} \rangle n_{i\downarrow} - \langle n_{i\downarrow} \rangle \langle n_{i\uparrow} \rangle. \quad (3)$$

Equation (3) shows that the spin-up electrons at site $i$ interact with the average density of spin-down electrons and the spin-down electrons at site $i$ interact with the average density of spin-up electrons. As a consequence, the initial many-body problem was reduced to the single - particle problem. However, with such mean-field approximation, there is only Hartree term invoked, therefore only the out-of-plane magnetic moments are calculated. In the current work, we take consideration both the in-plane and out-of-plane spin components. In this regard, the Fock term should be thus included along with the Hartree term, then Eq. (3) is rewritten as follows;

$$n_{i\uparrow} n_{i\downarrow} = \langle n_{i\downarrow} \rangle n_{i\uparrow} + \langle n_{i\uparrow} \rangle n_{i\downarrow} - \langle n_{i\downarrow} \rangle \langle n_{i\uparrow} \rangle$$
$$- \langle S_i^- \rangle S_i^+ - \langle S_i^+ \rangle S_i^- + \langle S_i^+ \rangle \langle S_i^- \rangle, \quad (4)$$

with $S_i^+ = a_{i\uparrow}^+ a_{i\downarrow}$ ($S_i^+ = b_{i\uparrow}^+ b_{i\downarrow}$) and $S_i^- = a_{i\downarrow}^+ a_{i\uparrow}$ ($S_i^- = b_{i\downarrow}^+ b_{i\uparrow}$).

By using the Fourier transformations, Eq. (1) is rewritten in the k-space;

$$H^{HF}(k) = \sum_{k\sigma} (a_{k\sigma}^+ b_{k\sigma}(-t\gamma_k) + b_{k\sigma}^+ a_{k\sigma}(-t\gamma_k^*))$$
$$+ \sum_k \lambda_k (a_{k\uparrow}^+ a_{k\uparrow} - a_{k\downarrow}^+ a_{k\downarrow} - b_{k\uparrow}^+ b_{k\uparrow} + b_{k\downarrow}^+ b_{k\downarrow})$$
$$+ \frac{U}{N} \sum_k (\langle n_{k\downarrow} \rangle n_{k\uparrow} + \langle n_{k\uparrow} \rangle n_{k\downarrow} - \langle n_{k\downarrow} \rangle \langle n_{k\uparrow} \rangle$$
$$- \langle S_i^- \rangle S_i^+ - \langle S_i^+ \rangle S_i^- + \langle S_i^+ \rangle \langle S_i^- \rangle). \quad (5)$$

Where,

$$\lambda_k = 2\lambda \left( -\sin(\sqrt{3} a k_y) + 2\cos\left(\frac{3}{2} a k_x\right) \sin\left(\frac{\sqrt{3}}{2} a k_y\right) \right),$$
$$\gamma_k = \sum_{n=1}^3 e^{-ik\delta_n},$$

with $\delta_1 = \left(\frac{a}{2}, \frac{a\sqrt{3}}{2}\right), \delta_2 = \left(\frac{a}{2}, -\frac{a\sqrt{3}}{2}\right)$ and $\delta_3 = (-a, 0)$.

Here, $a$ is the lattice constant of graphene and $\delta_n$ (n = 1 - 3) are the nearest-neighbor vectors. $N$ is the number of k-points.

The self-consistent algorithm with the convergence condition of $10^{-8}$ was used to deal with Eq. (5). Typically, randomly initial values of the spin-resolved densities were plugged in the $H^{HF}(k)$ matrix at the first step. The expectation values of the spin-resolved densities were computed from the eigenstates of $H^{HF}(k)$ matrix. These densities were then used as the initial values for next step. This procedure was repeated until satisfying convergence condition. Accomplishing the self-consistent computation, the in-plane ($M^{in}$) and out-of-plane ($M^{out}$) magnetic moments are calculated by the following equations;

$$M^{in} = \frac{\langle S_k^+ \rangle + \langle S_k^- \rangle}{2},$$
$$M^{out} = \frac{\langle n_{k\uparrow} \rangle + \langle n_{k\downarrow} \rangle}{2} \quad (6)$$

The energy dispersion is obtained from the computation,

$$E(k) = \pm\sqrt{-t^2 \gamma_k^2 + (\lambda_k - Um)^2 - U^2 n^2},$$

with $m = \frac{1}{2N} \sum_k (\langle n_{k\uparrow} \rangle - \langle n_{k\downarrow} \rangle)$ and $n = \frac{1}{N} \sum_k \langle S_k^\pm \rangle$. It can be seen that without Coulomb energy $U$ and SOC $\lambda_k$ the energy dispersion $E(k)$ reduces to the nearest-neighbor hopping tight-binding model with $E(k) = \pm t\gamma_k$ and then at the Dirac (or K) points, $E(K) = E(K') = 0$. Results obtained will be discussed in detailed in next section.

## 3. Results and discussion

The single-particle energy spectra of graphene with different parameters of $U$ and $\lambda$, are shown in Figure 1. As well-known, the infinite graphene reveals a zero bandgap and non-magnetism. The conduction band and valence band touch each other at the Dirac points, see Figure 1 (a), in good agreement with previous publishes [2, 9]. Such behavior maintains until the Coulomb energy applied greater than a Mott-Hubbard point [9, 24], an antiferromagnetic state is triggered with a finite bandgap, as shown Figure 1(b). By contrary, as the SOC is considered, a finite gap is always observed, as shown in Figure 2. Conspicuously, neglecting the $U$ and considering at the Dirac points, $E(K) = E(K') \sim \lambda$ therefore an infinitesimal $\lambda$ can be a nonzero gap. Our numerical calculations also indicated that the bandgap increases linearly with the increase of the $\lambda$ in the range from 0 to $1/3\sqrt{3}t$ and then it remains a constant, these results are in consistence with previous work [19]. However, it can be seen in Figure 2 the gap position shifts from the K point to the M point. Moreover, a bigger gap is observed as both $U$ and $\lambda$ are involved, typically $U = 2.5t$ and $\lambda = 0.1t$, see Figure 1c. The findings also were reported by the QMC calculations [18, 20]. The density of functional theory calculations indicated a small gap ($\sim 10^{-3}$ $meV$) in the graphene under the spin-orbit coupling [25]. Remarkably, the mirror symmetry of the energy spectrum is still preserved under the effect of the interaction considered here.
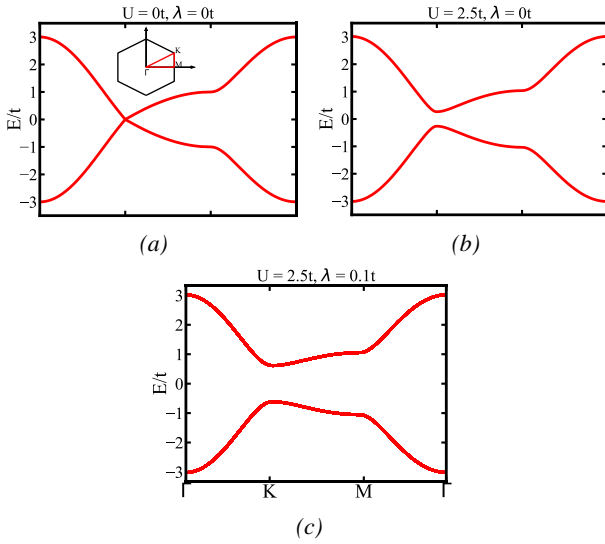
*(a)*



*(b)*



*(c)*

**Figure 1.** *Single-particle energy of the graphene honeycomb lattice with different parameters; (a) U = 0t, λ = 0t; (b) U = 2.5t, λ = 0t; (c) U = 2.5t, λ = 0.1t*
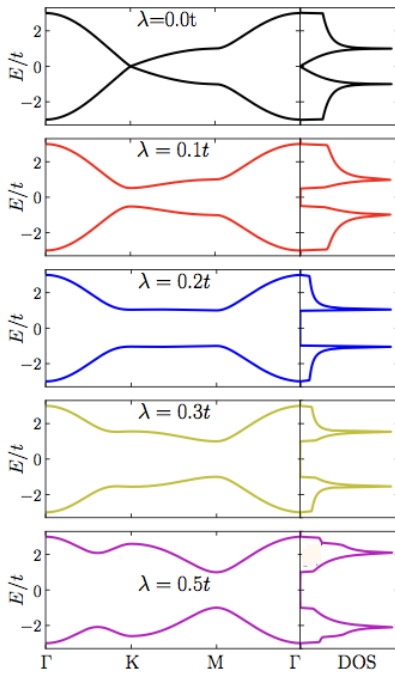


**Figure 2.** *Single-particle energy spectra (left) and density of state - DOS (right) for the graphene honeycomb lattice with different λ*
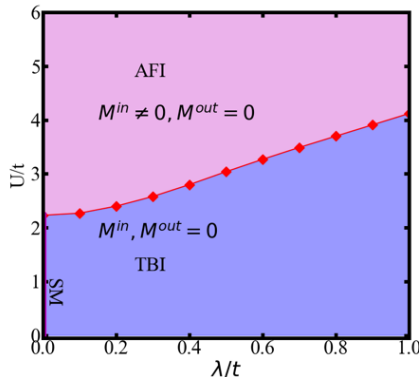


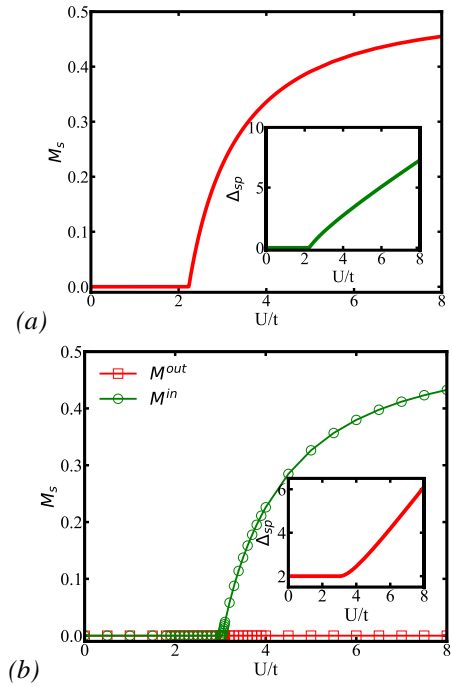**Figure 3.** *Phase diagram of graphene honeycomb lattice using the KMH model within the mean-field theory*



*(a)*



*(b)*

**Figure 4.** *Staggered magnetism and single-particle gap (inset) of graphene honeycomb lattice without (a) and with (b) spin-orbit coupling at λ = 0.5t*

The SOC-dependent magnetism is rendered in Figure 3. Within the mean-field Hartree - Fock approximation, three phases are observed including the gapless semi-metal (SM), topological band insulator (TBI) and antiferromagnetic insulator (AFI). More detailed, the SM state is characterized by zero bandgap and non-magnetization, and exists at zero SOC and weak Coulomb energy $U$. When $\lambda = 0$, a transition from the SM to AFI state occurs at $U \approx 2.23t$, revealed within the MFT level, which was reported in previous works [9]. The evolution of staggered magnetism ($M_s$) and single-particle gap ($\Delta_{sp}$) as a function of $U/t$ in the graphene honeycomb lattice were calculated and plotted in Figure 4 (a). Both $M_s$ and $\Delta_{sp}$ significantly increase with increasing $U/t$ in the AFI phase. Another transition from the SM to TBI phases appears with a finite SOC $\lambda$. This phase is characterized by the non-zero gap, as shown in the inset of Figure 4 (b) and Figure 3. Moreover, resembling in the SM phase, the spin moments in this phase do not polarized even though a weak Coulomb energy U is accounted. To achieve the antiferromagnetic state, a sufficiently large parameter U needs to be included, at least $U \approx 3t$ is required to turn on the spin polarization with $\lambda = 0.5t$, as an example (Figure 4(b)).

According to the phase diagram, the rise of the $\lambda$ magnitude results in getting larger $U$ in which occurs a transition to the AFI state. These values $U$ in the case including the SOC is obviously larger than that in the case without the SOC. Therefore, this result may cause by the presence of the nonzero bandgap. Most importantly, our calculation shows that the spin-orbit interaction suppresses the parallel orientation of magnetic moments to the z axis, $M^{out} = 0$ and it is prior to the development of *xy*-plane magnetic moments, $M^{in} \neq 0$. For more clearly, one can see in Figure 4(b), the $M^{out}$ (red squares) is completely

quenched, while the $M^{in}$ (green circles) is triggered at U≈ 3t and gets bigger as shifting to the higher Coulomb energy $U$. Similarly, the single-particle gap is a linear function of $U/t$. Noticeably, this result has not still represented in any articles yet.
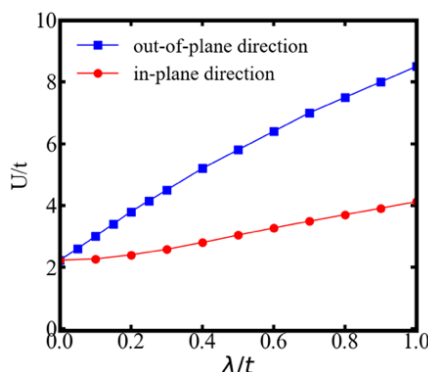


*Figure 5. Phase diagram using KMH model within the mean-field theory with different quantization axis choices*

Furthermore, we make a comparison between the phase diagram in Ref. [19] and our calculation, the results in Ref. [19] reproduced and plotted in Figure 5. Although both curves point out the increase of $U/t$ when the $\lambda/t$ rises, there is a big gap between two values $U/t$ at the same value of $\lambda/t$. This deviation stems from the choice of the quantization axis, typically, z-axis (out-of-plane direction) and x-axis (in-plane direction). For $\lambda = 0$, the critical point, $U_c \approx 2.23t$, does not depend on the quantization direction due to the conserve of the *SU(2)* symmetry. For $\lambda \neq 0$, the fact that the developing orientation of spin moments prefer the in-plane direction as mentioned above and according to other calculations like Quantum Monte Carlo simulations [20, 21], a stronger electron-electron interaction is thus required to onset the antiferromagnetic state in the out-of-plane direction. Therefore, the value of $U_c$ in the z-direction (blue squares) was overestimated, while that in the remaining direction (red circles) is underestimated. From above points, it can be deduced that our calculations shown here are more accurate than those published in Ref. [19] within Hartree-Fock approximation.

## 4. Conclusion

This study pointed out the influence of the intrinsic spin-orbit coupling on the spin polarization in the graphene honeycomb lattice. Within the KMH model combined to the Hartree-Fock approximation, a phase transition from topological insulator phase to antiferromagnetic insulator phase was observed rather than that from semi-metallic to antiferromagnetic phase without including the SOC. The computation results also elucidated the prior to the in-plane magnetic moment orientation in the presence of the SOC at the mean-field approximation. Furthermore away, the findings in this work contribute to further fundamental understanding in the 2D researching domain.

## REFERENCES

[1] K. Wakabayashi, K.I. Sasaki, T. Nakanishi and T. Enoki, "Electronic states of graphene nanoribbons and analytical solutions", *Science and Technology of Advanced Materials*, 11(5), 2010, 054504.

[2] A.H. Castro Neto, "The electronic properties of graphene", *Reviews of Modern Physics*, 81(1), 2009, 109.

[3] C.J. Bullock and C. Bussy, "Biocompatibility considerations in the design of graphene biomedical materials", *Advanced Materials Interfaces*, 2019, 1900229 (1-15).

[4] S.S. Gregersen, S.R. Power, A.P. Jauho, "Nanostructured graphene for spintronics", *Physical Review B*, 95, 2017, 121406.

[5] T.T. Phùng, R. Peters, A. Honecker, G.T de laissardière, J. Vahedi, "Spin-caloritronic transport in hexagonal graphene nanoflakes", *Physical Review B*, 102, 2020, 035160.

[6] S. Ganguly, M. Kabir, and T. Saha-Dasgupta, "Magnetic and electronic crossovers in graphene nanoflakes", *Physical Review B*, 95, 2017, 174419.

[7] W. Hu, Y. Huang, X. Qin, L. Lin, E. Kan, X. Li, C. Yang and J. Yang, "Room-temperature magnetism and tunable energy gaps in edge-passivated zigzag graphene quantum dots", *npj 2D Materials and Applications,* 3(17), 2019, (1-5).

[8] O.V. Yazyev, "Emergence of magnetism in graphene materials and nanostructure", *Reports on Progress in Physics*, 73, 2010, 056510.

[9] M. Raczkowski, R. Peters, T.T. Phùng, N. Takemori, F.F. Assaad, A. Honecker, and J. Vahedi, "The hubbard model on the honeycomb lattice: from static and dynamical mean-field theories to lattice quantum monte carlo simulations", *Physical Review B*, 101, 2020, 125103.

[10] G.Z. Magda, X.Z. Jin, I. Hagymasi, P. Vancsó, Z. Osváth, P. Nemes-Incze, C. Hwang, L.P. Biró, and L. Tapasztó, "Room-temperature magnetic order on zigzag edges of narrow graphene nanoribbons", *Nature*, 514, 2014, 608.

[11] J. Fernandez-Rossier, J.J. Palacios, "Magnetism in graphene nano-island", *Physical Review Letters,* 99, 2007, 177204.

[12] J.J. Palacios, J. Fernández-Rossier, and L. Brey, "Vacancy-induced magnetism in graphene and graphene ribbons", *Physical Review B*, 77, 2008, 195428.

[13] O.V. Yazyev and L. Helm, "Defect-induced magnetism in graphene", *Physical Review B*, 75, 2007, 125408.

[14] Q. Miao, L. Wang, Z. Liu, B. Wei, F. Xu, and W. Fei, "Magnetic properties of N-doped graphene with high Curie temperature", *Scientific Reports*, 6, 2016, 21832.

[15] S.L. Yu, X.C. Xie, and J.X. Li, "Mott physics and topological phase transition in correlated dirac fermions", *Physical Review Letters,* 107, 2011, 010401.

[16] C.L. Kane and E.J. Mele, "Quantum spin Hall effect in graphene", *Physical Review Letters,* 95, 2005, 226801.

[17] F.D.M. Haldane, "Model for a quantum Hall effect without Landau levels: Condensed-matter realization of the 'parity anomaly'", *Physical Review Letters,* 61, 1988, 2015.

[18] Z. Koinov, "Phase diagram of the attractive Kane-Mele-Hubbard model at half filling", *Atoms*, 8, 2020, 58.

[19] S. Rachel and K. le Hur, "Topological insulators and Mott physics from the Hubbard interaction", *Physical Review B*, 82, 2010, 075106.

[20] M. Bercx, M. Hohenadler, and F.F. Assaad, "Kane-Mele-Hubbard model on the $\pi$-flux honeycomb lattice", *Physical Review B*, 90, 2014, 075140.

[21] J.L. Lado, J. Fernandez-Rossier, "Magnetic edge anisotropy in graphene-like honeycomb crystal", *Physical Review Letters,* 113, 2014, 027203.

[22] W.H. Leong, S.L. Yu, J.X. Li, "Effects of the spin-orbit coupling on the vacancy-induced magnetism on the honeycomb lattice", *Physic Letters A*, 278, 2014, 2280 – 2284

[23] M. Luo, "Topological edge states of a graphene zigzag nanoribbon with spontaneous edge magnetism", *Physical Review B*, 102, 2020, 075421.

[24] H. Feldner, Z.Y. Meng, A. Honecker, D. Cabra, W. Stefan, F.F. Assaad, "Magnetism of finite graphene samples: Mean-field theory compared with Exact diagonalization and Quantum Monte Carlo simulation", *Physical Review B*, 81, 2010, 115416.

[25] Y. Yao, F. Ye, X.-L. Qi, S.-C. Zhang and Z. Fang, "Spin-orbit gap of graphene: First-principles calculations", *Physical Review B*, 75, 2007, 041401(R).